Breast Cancer Cells Exhibit Mesenchymal-Epithelial Plasticity Following Dynamic Modulation of Matrix Stiffness

Chinmay S. Sankhe, Jessica L. Sacco, Jacob Lawton, Ryan A. Fair, David Vidotto Rezende Soares, Mohammed K.R. Aldahdooh, Enrique D. Gomez, Esther W. Gomez *

C. S. Sankhe, J. Lawton, J.L. Sacco, D.V.R. Soares, E.D. Gomez, E.W. Gomez
Department of Chemical Engineering, The Pennsylvania State University, University Park, PA 16802, USA

R.A. Fair, E.D. Gomez
Department of Materials Science and Engineering, The Pennsylvania State University, University Park, PA 16802, USA

M.K.R. Aldahdooh
Department of Chemistry, The Pennsylvania State University, University Park, PA 16802, USA

E.W. Gomez
Department of Biomedical Engineering, The Pennsylvania State University, University Park, PA 16802, USA
Email: ewg10@psu.edu

Keywords: Hyaluronic acid, integrin-linked kinase, apoptosis, breast cancer, extracellular matrix

Mesenchymal-epithelial transition (MET) is essential for tissue and organ development and is thought to contribute to cancer by enabling the establishment of metastatic lesions. Despite its importance in both health and disease, there is a lack of *in vitro* platforms to study MET and little is known about the regulation of MET by mechanical cues. Here, hyaluronic acid-based hydrogels with dynamic and tunable stiffnesses mimicking that of normal and tumorigenic mammary tissue were synthesized. The platform was then utilized to examine the response of mammary epithelial cells and breast cancer cells to dynamic modulation of matrix stiffness. Gradual softening of the hydrogels reduces proliferation and increases apoptosis of breast cancer cells. Moreover, breast cancer cells exhibit temporal changes in cell morphology, cytoskeletal organization, and gene expression that are consistent with mesenchymal-epithelial plasticity as the stiffness of the matrix is reduced. A reduction in matrix stiffness attenuates expression of integrin linked kinase, and inhibition of integrin linked kinase impacts

proliferation, apoptosis, and gene expression in cells cultured on stiff and dynamic hydrogels. Overall, these findings reveal intermediate epithelial/mesenchymal states as cells move along a matrix stiffness mediated MET trajectory and suggest an important role for matrix mechanics in regulating mesenchymal-epithelial plasticity.

1. Introduction

Mesenchymal-epithelial transition (MET) is a dynamic phenotypic change in which migratory, spindle shaped cells with front-rear polarity and weak cell-cell contacts transition to assemblies of cells exhibiting apicobasal polarity and stable epithelial cell-cell adhesions. MET is an important process that occurs during development and is central to embryonic remodeling and establishment of organ architecture.[1] Beyond embryogenesis, MET is thought to contribute to cancer progression by enabling the establishment of distant metastases and to reprogramming of somatic cells into induced pluripotent stem cells.[1-2] Investigations of MET processes have mainly focused on the impact of biochemical cues in embryogenesis and *in vivo* animal models of cancer metastasis.[2a, 2i, 3] These systems can be difficult to control, and it can be challenging to decouple the effects of different types of signals on cell response. Consequently, little is known about how physical parameters regulate MET.

A number of findings suggest that mechanical signals may guide the steps of MET. The mechanical properties of the cellular niche change dynamically during MET-associated processes *in vivo* including embryonic development,[4] wound healing,[5] and disease progression.[2i, 6] Biophysical factors including tissue geometry,[7] matrix stiffness,[8] cyclic stretch,[9] and cell contractility[10] are also known to control epithelial-mesenchymal transition (EMT). MET has classically been described as a symmetrical reversion of EMT, however, some studies indicate that during development MET and EMT may be controlled by different mechanisms and may not simply be reverse processes.[11] It is likely that MET and EMT exhibit distinct kinetics and trajectories and therefore may be differentially regulated by mechanical cues.[12] Furthermore, *in vivo* studies have shown re-expression of epithelial markers in tumor metastases from E-cadherin-negative tumor cell xenografts and elevated levels of E-cadherin in lymph node metastases when compared to primary tumors,[2d, 2f] both of which indicate that MET may contribute to secondary tumor formation. The mechanical properties of distant metastatic sites can differ significantly from those of the primary tumor niche and may therefore influence MET. In addition, the mechanical properties of the primary tumor niche change dynamically during tumor progression,[6b] which can promote EMT. Several studies suggest

that targeting or downregulating EMT in tumor-initiating cells can reduce migration and invasion of cancer cells, thereby reducing metastatic potential.[13] However, whether targeting the mechanics of the extracellular matrix can promote loss of a mesenchymal and gain of an epithelial phenotype in cancer cells at primary tumor sites is not known. The complex nature of animal models and embryos that have been used to study MET makes it difficult to delineate the role of mechanics in regulating mesenchymal-epithelial plasticity. Thus, new model systems are necessary in which one can control the biochemical and biophysical properties of the cellular microenvironment thereby enabling systematic studies of the impact of environmental cues such as matrix stiffness on cell plasticity and MET.

The effect of matrix stiffness on EMT has been extensively studied primarily through the use of hydrogels with static mechanical properties.[8a-c, 14] Few *in vitro* studies have examined the role of matrix stiffness in the regulation of MET.[15] Many of these studies have focused on endpoint analysis of EMT and lack details regarding the dynamics of cell transitions in response to mechanical cues. Materials with dynamic control of stiffness have the potential to enable examination of cell transitions through hybrid epithelial/mesenchymal states and elucidation of the underlying molecular mechanisms governing cellular processes in a way that cannot be achieved in static systems. A variety of biomaterials including hyaluronic acid (HA), sodium alginate, poly(ethylene glycol), and azobenzene have been used to fabricate cell culture platforms that can undergo changes in stiffness as a function of time.[16] Methacrylated HA (MeHA) in particular has been previously employed to create a hydrogel platform that can be dynamically stiffened to examine EMT.[17] Furthermore, MeHA crosslinked with dithiothreitol (DTT) and pentaerythritol tetrakis(mercaptoacetate) (PETMA) has also been used to fabricate a hydrogel platform that undergoes gradual softening to monitor hepatic stellate cell response.[18] Given that HA is a component of the tumor microenvironment[19] and elevated HA production[20] and stiffening of the extracellular matrix[8a-c, 17b] are associated with EMT, an HA-based hydrogel that softens with time may be a useful model system for examining mesenchymal-epithelial plasticity.

In this work, we develop an *in vitro* MeHA-based hydrogel platform with stiffnesses that are tuned to mimic the mechanical properties of normal and tumorigenic breast tissue. Using a combination of stable and hydrolytically degradable crosslinkers, we create hydrogels with static and dynamic matrix stiffness and utilize this platform to examine mesenchymal-epithelial plasticity in mammary epithelial cells and breast cancer cells. Breast cancer cells cultured on

stiff hydrogels show increased cell spreading and elongation, lamellipodia formation, proliferation, and expression of mesenchymal markers in comparison to cells cultured on soft hydrogels. When cells are cultured on dynamic hydrogels, gradual lowering of matrix stiffness promotes a reduction in cell elongation, proliferation, and expression of mesenchymal markers and reveals an increase in the expression of epithelial markers as well as apoptosis in breast cancer cells. Furthermore, the expression of integrin-linked kinase (ILK), a signaling molecule that regulates cell proliferation, apoptosis, and differentiation, decreases with time as the matrix softens. Inhibition of ILK activity attenuates mesenchymal phenotypic characteristics including cell spreading, elongation, and expression of the mesenchymal marker vimentin. Together, these findings reveal intermediate epithelial/mesenchymal states as cells move along a matrix stiffness mediated MET trajectory. Overall, our results suggest an important role for mechanical signals in regulation of mesenchymal-epithelial plasticity.

2. Results

2.1. Synthesis of MeHA hydrogels with static and dynamic mechanical properties that mimic normal and tumorigenic mammary tissue

The extracellular matrix experiences dynamic mechanical, structural, and compositional changes during breast cancer progression.[6b, 21] Increased expression of HA in the tumor microenvironment is associated with breast cancer malignancy and poor patient prognosis[19] and increased production of HA can promote EMT in normal epithelial cells.[20] Furthermore, increased matrix stiffness can promote EMT;[8b, 8c] however, little is known about the impact of HA and matrix mechanical properties on MET, particularly in breast cancer cells. Here, we fabricated an HA-based hydrogel platform to determine whether changes in the mechanical properties of the matrix can promote MET in breast cancer cells. HA was chemically modified using methacrylic anhydride to form methacrylated hyaluronic acid (MeHA; **Figure S1**). MeHA can be crosslinked by chemical and photo- initiators to create hydrogels with defined mechanical properties. We synthesized MeHA hydrogels using 2 w/v% MeHA that was crosslinked with the photo-initiator Irgacure (0.05 w/v%) which forms stable crosslinks in the presence of ultraviolet (UV) light. Atomic force microscopy was used to evaluate the mechanical properties of the hydrogels and representative modulus maps are shown in **Figure S2**. Increasing the UV exposure time enhances the Young's modulus of the hydrogel (**Figure 1a**). A UV exposure time of 15 sec produces a hydrogel with a modulus of 210 Pa which mimics the mechanical properties of normal mammary tissue while an exposure time of 65 sec produces a hydrogel with a modulus of 2100 Pa that mimics the stiffness of an average breast tumor.[6b,

[21] No significant differences are observed for the Young's moduli of the MeHA hydrogels crosslinked with Irgacure when comparing moduli between the day of synthesis (day 0) and 21 days later (**Figure S3**), suggesting that the mechanical properties of the hydrogels are stable as a function of time. We term MeHA hydrogels with stable Irgacure crosslinks as static hydrogels for this work.

To synthesize a dynamic hydrogel with a stiffness that gradually decreases with respect to time, pentaerythritol tetrakis(3-mercaptopropionate) (PETMP), a tetrafunctional crosslinker that can form thiol linkages with MeHA, was incorporated into hydrogels simultaneously with Irgacure. PETMP can undergo gradual hydrolysis which reduces hydrogel crosslinking and stiffness as a function of time. As shown in **Figure 1b**, the Young's modulus of the hydrogels varies as a function of time, with a modulus of 1800 Pa on the day of synthesis (day 0) and a modulus of 310 Pa on day 21. Young's moduli of the hydrogel system as a function of time are listed in **Table S1**. Together, these data demonstrate that static and dynamic HA-based hydrogels can be tuned to mimic the mechanical properties of normal and tumorigenic mammary tissue.

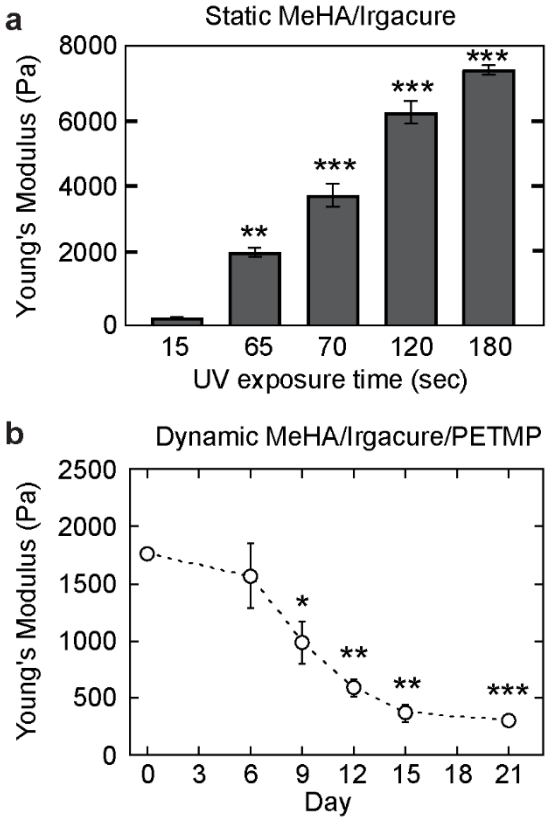

Figure 1. Mechanical characterization of methacrylated hyaluronic acid (MeHA)-based hydrogels. a) Young's modulus of static MeHA/Irgacure-based hydrogels as a function of increasing UV exposure time. Static soft (210 Pa) and stiff (2100 Pa) hydrogels correspond to UV exposure times of 15 and 65 sec, respectively. Data indicate mean ± sem for n=3 hydrogel

samples. **p<0.01, ***p<0.001 in comparison to the 15 sec UV exposure time hydrogel, evaluated using analysis of variance (ANOVA) followed by Tukey's post-hoc test. b) Young's modulus of dynamic MeHA/Irgacure/PETMP-based hydrogels as a function of time. Data indicate mean ± sem for n=3 hydrogel samples. *p<0.05, **p<0.01, ***p<0.001 in comparison to the day 0 sample, evaluated using analysis of variance (ANOVA) followed by Tukey's post-hoc test.

2.2. Breast cancer cells exhibit a change in cell morphology and cytoskeletal organization when cultured on MeHA hydrogels that soften with time

Cells undergo dramatic changes in morphology during EMT with a transition from a rounded, cuboidal shape to an elongated morphology.[7b] Culture of mammary epithelial cells on soft hydrogels renders the cells refractive to EMT-induced morphological changes while cells cultured on stiff hydrogels are permissive to EMT.[8c] Hence, we hypothesized that dynamically lowering matrix stiffness will induce morphological changes in breast cancer cells indicative of a MET-like response.

Increased levels of fibronectin are found in the extracellular matrix surrounding breast tumors in comparison to normal mammary tissue,[22] and fibronectin has been shown to stimulate EMT in mammary epithelial cells and breast cancer cells.[23] Thus, to model the breast tumor microenvironment we functionalized static and dynamic HA hydrogels with fibronectin and monitored cell morphology as a function of time. MDA-MB-231 breast cancer cells exhibit a spread and elongated morphology when cultured on static 2100 Pa hydrogels, indicative of a more mesenchymal-like phenotype (**Figure 2a**). In contrast, the cells remain rounded and less spread on static 210 Pa hydrogels. When cultured on the dynamic stiff-to-soft hydrogels, the MDA-MB-231 breast cancer cells initially exhibit a spread and elongated morphology similar to when cultured on the 2100 Pa hydrogels, and they show a decrease in cell spreading and elongation as a function of time as the hydrogel softens. Quantification of the cell spread area and aspect ratio (elongation) revealed that the cells maintain these morphological characteristics when cultured on both the static 210 Pa and 2100 Pa hydrogels for the span of 21 days (**Figure 2b,c**). Contrarily, cells cultured on the dynamic hydrogels show significantly reduced spread area and aspect ratio as a function of time. The impact of MeHA hydrogel mechanics on the less invasive MCF7 breast cancer cell line was also monitored. Similar trends in cell spread area and aspect ratio are observed when cultured on fibronectin-functionalized hydrogels in comparison to the MDA-MB-231 cells (**Figure S4**).

Collagen I in the tumor microenvironment also contributes to breast cancer initiation and progression.[24] Previous studies have functionalized MeHA hydrogels with collagen I to study the effect of matrix stiffness on induction of EMT in mammary epithelial cells.[17b] To test the impact of collagen I in our system, we functionalized static and dynamic MeHA hydrogels with collagen I to examine its impact on cell morphology as the matrix softens. MDA-MB-231 cells cultured on the collagen I-coated MeHA hydrogels exhibit similar trends in cell spread area and aspect ratio to when cultured on the fibronectin functionalized hydrogels (**Figure S5**). The cells spread and exhibit an elongated shape at early time points on the dynamic hydrogel, and as the hydrogel softens with time the cell morphology transitions to a rounded shape with more cell-cell interactions. Together, these observations suggest that dynamically reducing matrix stiffness induces a change in the morphological properties of breast cancer cells when cultured on matrix components found within the tumor microenvironment. The experiments within this study will further examine the impact of fibronectin functionalized hydrogels on mesenchymal-epithelial plasticity.

Mesenchymal cells can exhibit filopodia and lamellipodia that aid in migration and invasion[25] while epithelial cells typically display cortical actin structures.[26] Hence, we probed breast cancer cells with fluorescently tagged phalloidin to examine actin architecture. For MDA-MB-231 breast cancer cells, F-actin staining revealed that cells cultured on static 2100 Pa hydrogels exhibit stress fibers, filopodial protrusions, and lamellipodial structures, which are observed across 15 days of culture (**Figure 3**). In contrast, cells cultured on static 210 Pa hydrogels exhibit cortical actin localized primarily to the cell periphery and cell-cell borders. When the MDA-MB-231 cells are cultured on dynamic stiff-to-soft hydrogels, cells initially exhibit lamellipodial and filopodial structures and as the hydrogel gradually softens the actin organization shifts to a cortical structure. Similar trends in actin organization are observed in MCF7 cells (**Figure S6**). These data show that dynamic modulation of matrix stiffness can induce changes in actin cytoskeletal organization in breast cancer cells.

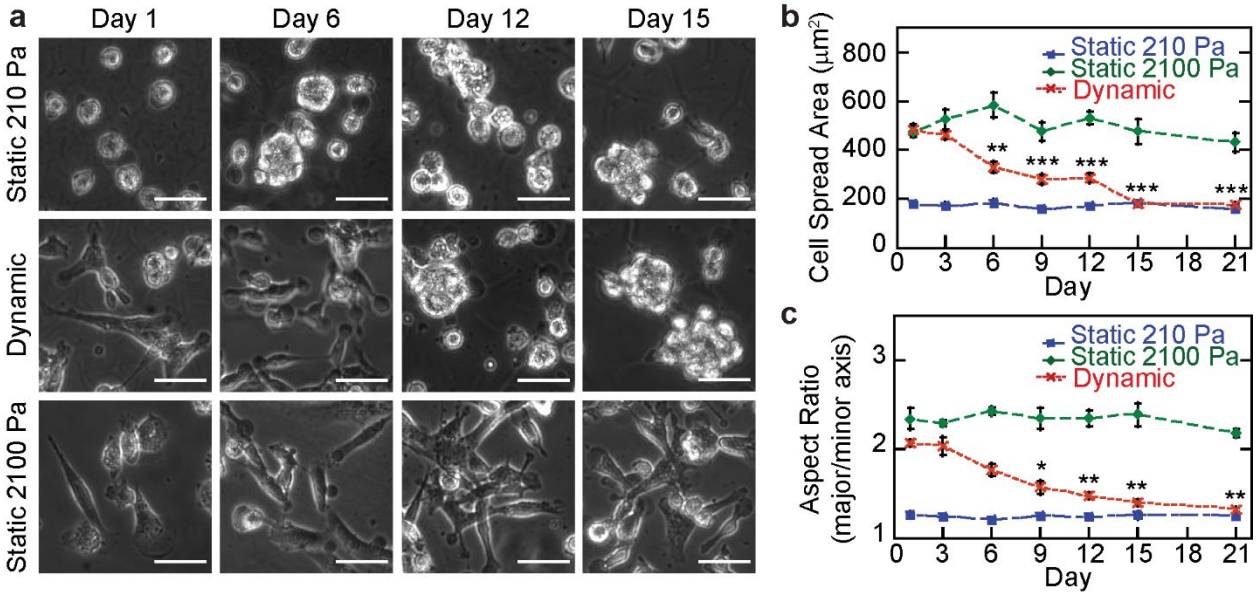

Figure 2. Dynamic softening of fibronectin-functionalized MeHA-based hydrogels promotes a change in the morphology of MDA-MB-231 breast cancer cells**.** a) Phase contrast microscopy images of MDA-MB-231 breast cancer cells cultured on static 210 Pa and 2100 Pa MeHA-based hydrogels and dynamic MeHA-based hydrogels and monitored as a function of time. Scale bars: 50 μm. Quantification of cell b) spread area and c) aspect ratio for MDA-MB-231 breast cancer cells cultured on different hydrogels and monitored for 21 days. At least 65 cells were quantified for every hydrogel group per trial. Data indicate mean ± sem for n = 3 trials. *p<0.05, **p<0.01, ***p<0.001 in comparison to day 1 and 3 time points of the dynamic hydrogel, evaluated using analysis of variance (ANOVA) followed by Tukey's post-hoc test.

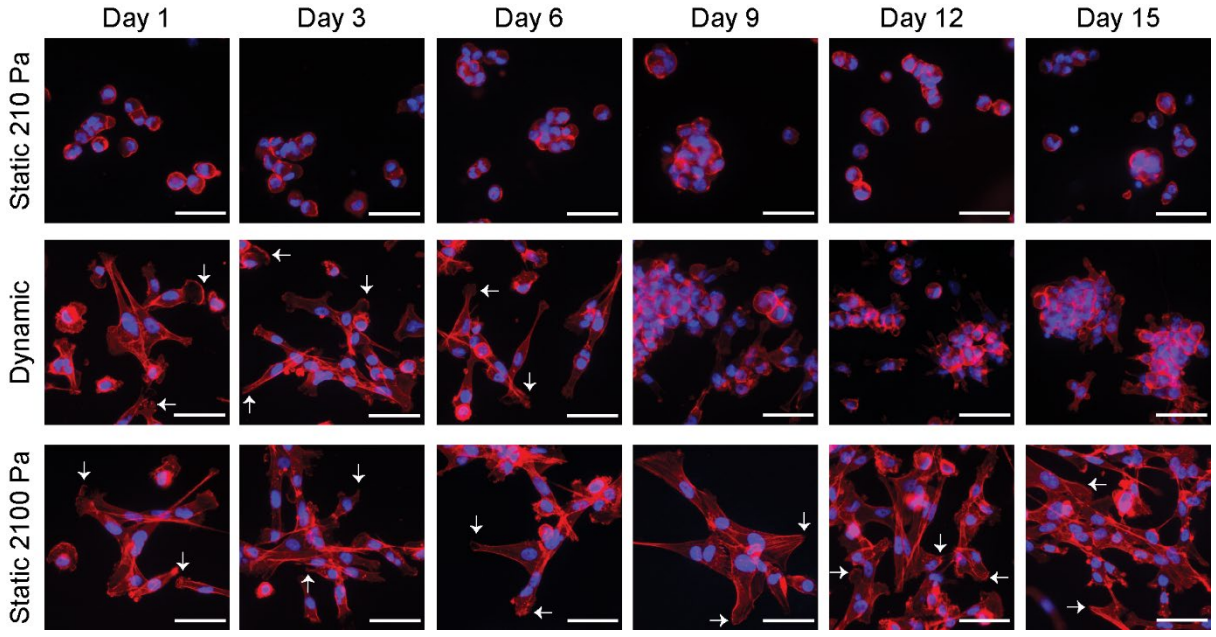

Figure 3. Dynamic softening of fibronectin-functionalized MeHA-based hydrogels promotes cytoskeletal reorganization in MDA-MB-231 breast cancer cells. F-actin staining using fluorescently-tagged phalloidin (red) in MDA-MB-231 breast cancer cells cultured on static 210 Pa and 2100 Pa MeHA-based hydrogels and dynamic MeHA-based hydrogels and monitored as a function of time. Nuclei are shown in blue. The white arrows indicate lamellipodial or filopodial structures. Scale bars: 50 μm.

2.3. Dynamic softening of the matrix induces apoptosis and attenuates proliferation in breast cancer cells

An increase in extracellular matrix stiffness reduces apoptosis, which can potentially help cancer cells to evade therapeutic measures.[27] Hence, we posited that dynamic changes in matrix stiffness may regulate apoptosis in breast cancer cells, with gradual lowering of the stiffness promoting apoptosis. We employed immunofluorescence staining to probe for the apoptotic protein marker cleaved caspase-3 in MDA-MB-231 breast cancer cells cultured on MeHA hydrogels with static and dynamic mechanical properties. For cells cultured on static 210 Pa hydrogels, the percentage of cells staining positive for cleaved caspase-3 was ~20%. The value appears to increase throughout the 15-day time period, but this change is not significant (**Figure 4a,b** and **Figure S7a**). On the other hand, for cells cultured on static 2100 Pa hydrogels, the percentage of cells staining positive for cleaved caspase-3 was approximately two-fold lower than for cells cultured on the 210 Pa hydrogels. When cultured on dynamic stiff-to-soft hydrogels, the percentage of cells that stained positive for cleaved caspase-3 was initially low, but it significantly increased over the 15-day time period as the matrix softened, with the percentage of cells positive for cleaved caspase-3 reaching similar levels to that in cells cultured on 210 Pa hydrogels. These observations suggest that dynamic softening of the matrix can induce increased apoptosis in breast cancer cells.

In addition to apoptosis, we also monitored breast cancer cell proliferation as a function of time and gradual softening of the hydrogel. Using immunofluorescence staining, we probed for the proliferation marker Ki67 in MDA-MB-231 breast cancer cells cultured on different MeHA hydrogels. For cells cultured on static 2100 Pa hydrogels, the percentage of cells staining positive for Ki67 was approximately 60%, which is roughly 2.5 to 3-fold higher than for cells cultured on the 210 Pa hydrogels (**Figure 4c,d** and **Figure S7b**). When cultured on dynamic stiff-to-soft hydrogels, the percentage of Ki67-positive cells was high initially, but it gradually decreased over the 15-day time period as the hydrogel softened. These observations suggest that dynamic softening of the matrix can attenuate proliferation in breast cancer cells.

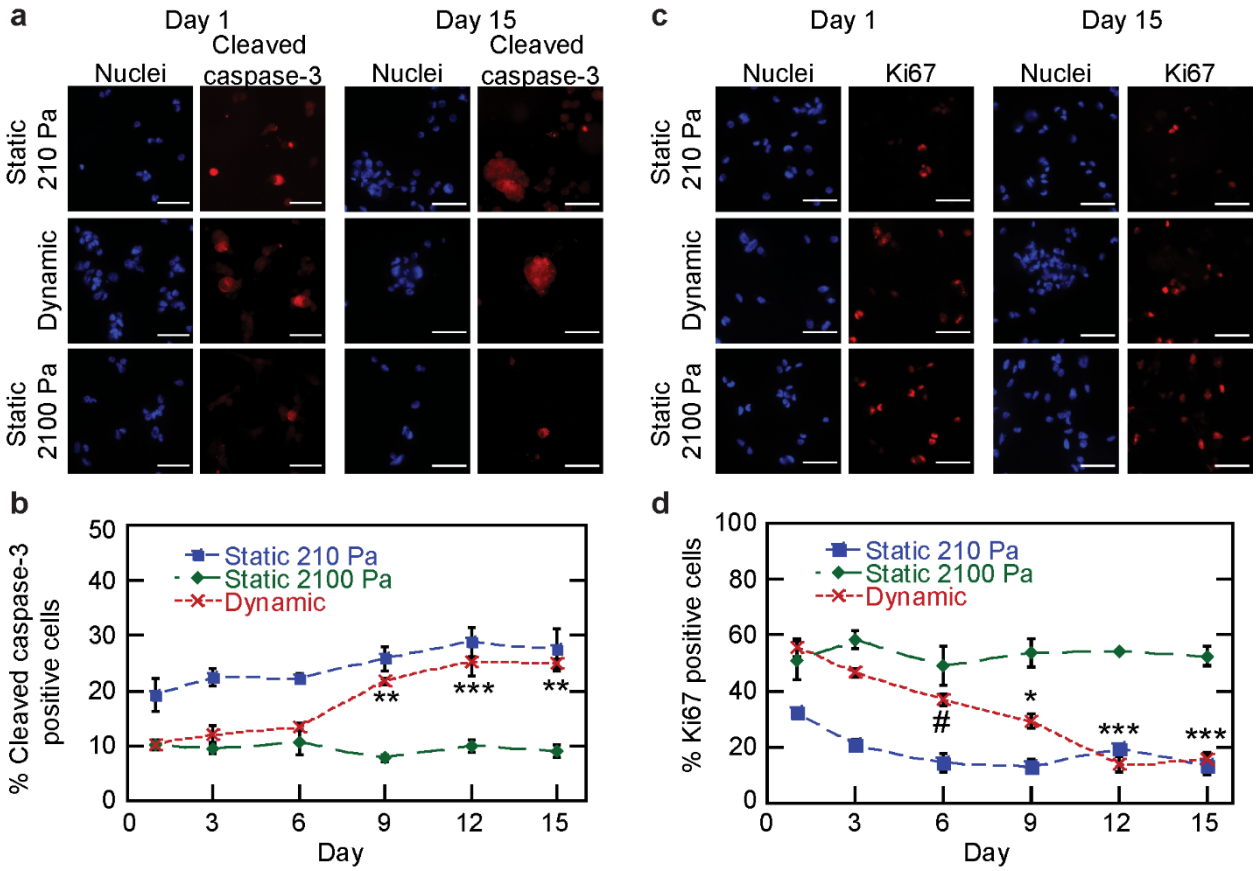

Figure 4. Softening of MeHA-based hydrogels induces apoptosis and attenuates proliferation in MDA-MB-231 breast cancer cells. Immunofluorescence staining and quantification of the percentage of cells staining positive for a,b) cleaved caspase-3 and c,d) Ki67 in MDA-MB-231 breast cancer cells cultured on static 210 Pa and 2100 Pa MeHA-based hydrogels and dynamic MeHA-based hydrogels and monitored as a function of time. Scale bars: 50 µm. At least 100 cells were quantified for every hydrogel group per trial. Data indicate mean ± sem for n=3 trials. For cleaved caspase-3, $^{**}p<0.01$, $^{***}p<0.001$ compared to day 1 sample of dynamic MeHA hydrogel. For Ki67, $^{*}p<0.05$, $^{***}p<0.001$ compared to day 1 and day 3 sample of dynamic MeHA hydrogel, $^{\#}p<0.01$ compared to day 1 of dynamic MeHA hydrogel, evaluated using analysis of variance (ANOVA) followed by Tukey's post-hoc test.

2.4. Dynamic softening of the matrix modulates the expression of epithelial and mesenchymal protein markers in breast cancer cells

Given that an increase in matrix stiffness can regulate changes in gene expression in normal mammary epithelial cells[8c] and cancer cells during EMT,[14-15] we hypothesized that gradual softening of the matrix may impact the expression of mesenchymal and epithelial markers in mammary epithelial cells and breast cancer cells. Co-staining of MCF10A mammary epithelial cells for E-cadherin and vimentin revealed low vimentin levels and localization of E-cadherin to cell-cell contacts in cells cultured on static 210 Pa hydrogels (**Figure 5**). In contrast, MCF10A cells cultured on static 2100 Pa hydrogels show high levels of vimentin and low levels of E-cadherin across all time points. When cultured on the dynamic stiff-to-soft hydrogels,

MCF10A cells show high vimentin and low E-cadherin levels at early times and as the matrix softens vimentin expression decreases and E-cadherin localization to cell-cell contacts increases.

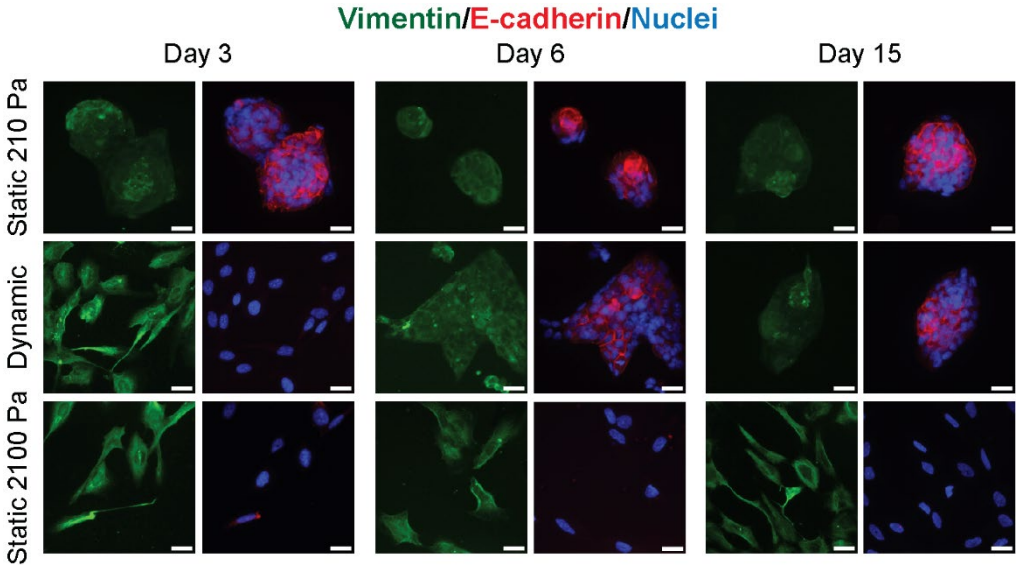

Figure 5. Immunofluorescence staining for E-cadherin (red) and vimentin (green) in MCF10A mammary epithelial cells cultured on static and dynamic fibronectin functionalized MeHA hydrogels. Scale bars: 25 μm.

For MDA-MB-231 breast cancer cells cultured on static 210 Pa hydrogels, immunofluorescence staining for vimentin shows localization to regions surrounding the nucleus, while for cells cultured on static 2100 Pa hydrogels, vimentin fibers are found throughout the cytoplasm, and in some cells, also extend to the cell periphery (**Figure 6a**). For MDA-MB-231 cells cultured on dynamic stiff-to-soft hydrogels, immunofluorescence staining revealed that vimentin fibers extend throughout the cytoplasm up to day 6 and later switch to primarily surrounding the nucleus at later times. Studies have shown that MDA-MB-231 breast cancer cells do not express E-cadherin,[28] and the loss of E-cadherin expression in these cells is attributed to hypermethylation of CpG islands at the E-cadherin promoter.[29] In addition, for many breast cancer cells, elevation of H3K9 tri-methylation at the E-cadherin promoter leads to its repression.[30] To examine whether matrix softening can induce E-cadherin expression in MDA-MB-231 cells, we performed immunofluorescence staining to monitor E-cadherin expression and localization (**Figure S8a**). MDA-MB-231 cells cultured on static 2100 Pa substrates do not form cell-cell contacts or exhibit E-cadherin expression. When the MDA-MB-231 cells are cultured on static 210 Pa hydrogels, they do form cell-cell contacts, however, only a few cell clusters stain positive for E-cadherin. On the other hand, for cells cultured on dynamic

stiff-to-soft hydrogels, cells do not form cell-cell contacts nor stain positive for E-cadherin up to the day 6 time point. As the matrix softens, the cells form cell-cell contacts, and some cell clusters stain positive for E-cadherin (**Figure S8a**).

To confirm these observations, we performed western blotting for E-cadherin in MDA-MB-231 cells on different MeHA hydrogels, but the expression of E-cadherin was not detected (**Figure 6b**). When MDA-MB-231 cells are cultured on dynamic stiff-to-soft hydrogels, the expression levels of mesenchymal protein markers vimentin and fibronectin decrease for time points later than 6 days as the matrix softens (**Figure 6b-d**). For the epithelial marker pan-cytokeratin, a significant increase in expression is observed at day 15 in comparison to the earlier time points that were analyzed (**Figure 6b,e**). We also monitored the expression of these markers in MDA-MB-231 breast cancer cells cultured on static 210 Pa and 2100 Pa hydrogels as a function of time. The expression levels of vimentin and fibronectin increase in cells cultured on static 2100 Pa hydrogels as a function of time and are in general higher than the expression levels of these markers in cells cultured on the static 210 Pa hydrogels (**Figure S9a-c**). No significant differences are seen in the expression levels of pan-cytokeratin as a function of time for MDA-MB-231 cells cultured on the static 210 Pa and 2100 Pa hydrogels (**Figure S9a,d**). These data demonstrate that protein expression in MDA-MB-231 cells varies between static and dynamic hydrogels. Further studies are needed to examine regulation of E-cadherin expression as well as other mesenchymal and epithelial markers in these cells.

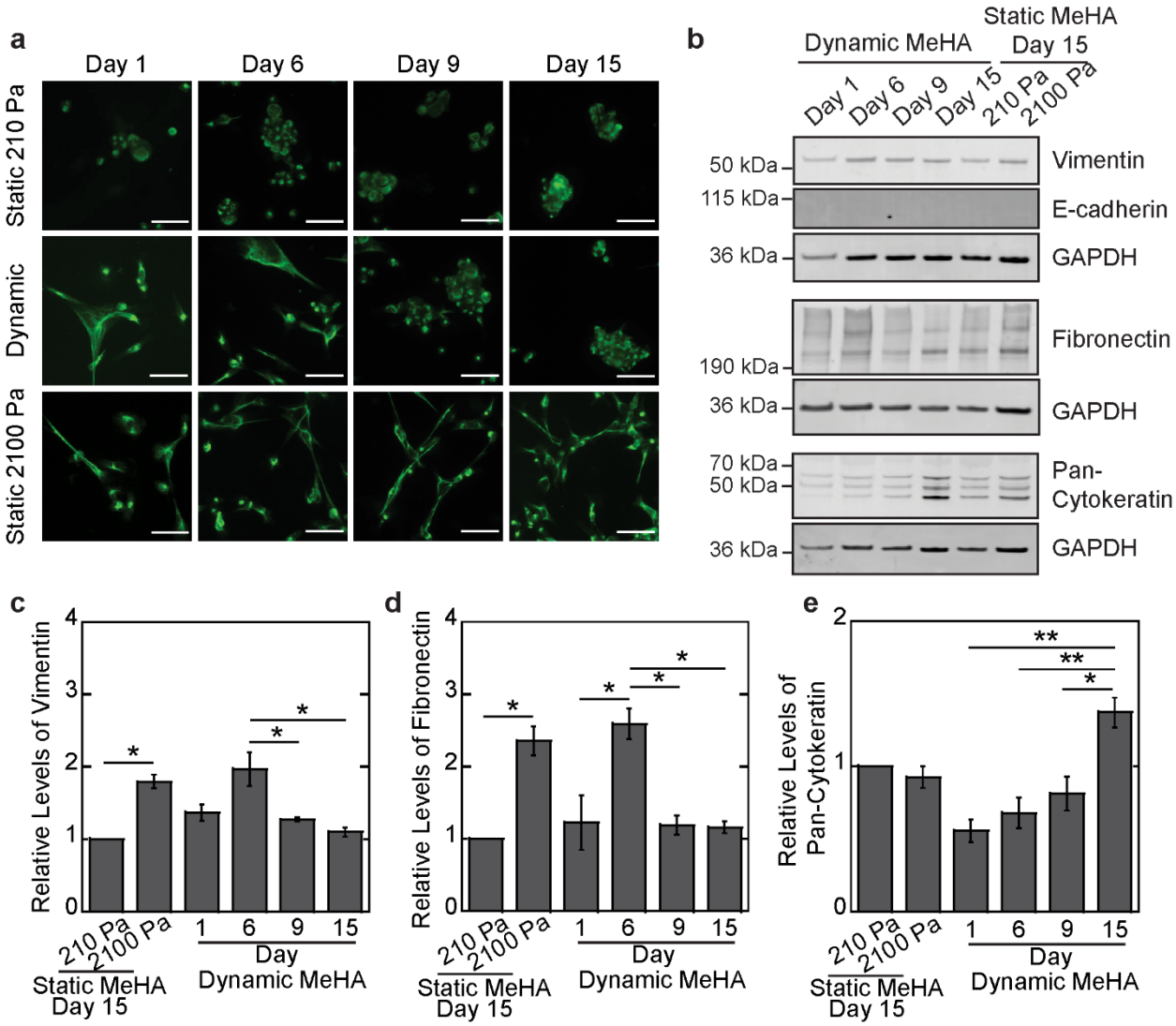

Figure 6. Dynamic softening of MeHA-based hydrogels regulates the expression of epithelial and mesenchymal markers in MDA-MB-231 breast cancer cells. a) Immunofluorescence staining images of vimentin in MDA-MB-231 breast cancer cells cultured on static 210 Pa and 2100 Pa MeHA-based hydrogels and dynamic MeHA-based hydrogels and monitored as a function of time. Scale bars: 50 μm. b) Western blotting for mesenchymal protein markers vimentin and fibronectin and epithelial protein markers E-cadherin and pan-cytokeratin in MDA-MB-231 breast cancer cells cultured on static and dynamic MeHA-based hydrogels. Densitometric analysis of c) vimentin, d) fibronectin, and e) pan-cytokeratin in MDA-MB-231 breast cancer cells cultured on static and dynamic MeHA-based hydrogels. Data normalized with respect to static MeHA 210 Pa day 15 sample. Data indicate mean ± sem for n = 3 trials. *$p<0.05$, **$p<0.01$, evaluated using the analysis of variance (ANOVA) followed by Tukey's post-hoc test.

We also examined the expression of epithelial and mesenchymal markers in MCF7 breast cancer cells. MCF7 cells express the epithelial marker E-cadherin[31] and do not express the mesenchymal marker vimentin.[32] Immunofluorescence staining revealed that when cultured on static 210 Pa hydrogels, MCF7 cells show E-cadherin localization at cell-cell junctions for

all time points monitored (**Figure S8b**). When cultured on static 2100 Pa hydrogels, MCF7 cells show reduced localization of E-cadherin to cell-cell junctions in comparison to cells cultured on the static 210 Pa hydrogels and exhibit mixed expression with some cells showing reduced levels of E-cadherin. On the dynamic stiff-to-soft hydrogels, cells show reduced E-cadherin localization to cell-cell junctions at early time points in comparison to later times (**Figure S8b**).

Protein marker levels were also monitored in MCF7 cells using western blotting. When cultured on dynamic stiff-to-soft hydrogels, the expression levels of epithelial markers E-cadherin and pan-cytokeratin increase at day 15, when the stiffness of the hydrogel is low, in comparison to the earlier time points (**Figure S10a-c**). While the expression level of the transcription factor Snail trends downward from day 6 to 15 as the matrix softens, differences are not significant (**Figure S10a,d**). On the other hand, the expression of fibronectin significantly decreases as the stiffness of the hydrogel is gradually lowered (**Figure S10a,e**). On hydrogels with static mechanical properties, the MCF7 cells show higher levels of E-cadherin and pan-cytokeratin expression when cultured on the 210 Pa hydrogels in comparison to on the 2100 Pa hydrogels across most time points (**Figure S10f-h**). Snail expression is significantly higher in cells cultured on 2100 Pa hydrogels in comparison to 210 Pa for days 6 and later (**Figure S10f,i**). Furthermore, fibronectin levels are also higher in MCF7 cells cultured on 2100 Pa hydrogels in comparison to 210 Pa hydrogels (**Figure S10f,j**). Together, the observations in MDA-MB-231, MCF7, and MCF10A cells suggest that a reduction in matrix stiffness as a function of time promotes downregulation of some mesenchymal markers and upregulation of epithelial markers indicative of mesenchymal-epithelial plasticity.

2.5. Breast cancer cells modulate the expression of integrin-linked kinase in response to a dynamic reduction in matrix stiffness

Cells adhere to extracellular matrix proteins including fibronectin and collagen I using integrins.[33] Integrins mediate force sensing with downstream signaling molecules such as integrin linked kinase (ILK) playing critical roles in mechanotransduction.[34] ILK, which binds to the cytoplasmic tails of β1 and β3 integrins,[35] regulates many cellular processes including growth, apoptosis, and differentiation[36] and has been shown to regulate a stiffness-induced switch between EMT and apoptosis.[37] We performed western blotting to monitor the expression of ILK1 in MDA-MB-231 breast cancer cells as a function of time when the cells were cultured on hydrogels with static and dynamic mechanical properties. Densitometric

quantification of the blots revealed that when the MDA-MB-231 cells were cultured on the dynamic stiff-to-soft hydrogels, the levels of ILK1 decrease as a function of time as the matrix softens (**Figure 7a,b**). When cells are cultured on MeHA hydrogels with static mechanical properties, the levels of ILK are higher in cells cultured on the 2100 Pa hydrogels in comparison to when cells are cultured on the 210 Pa hydrogels for all time points analyzed except for day 1 (**Figure 7c,d**). Moreover, the levels of ILK1 remain nearly constant in cells cultured on both static 210 Pa and static 2100 Pa hydrogels as a function of time. These data suggest that gradual lowering of the stiffness of the matrix promotes a reduction in the levels of ILK, which may regulate mesenchymal-epithelial plasticity, proliferation, and apoptosis.

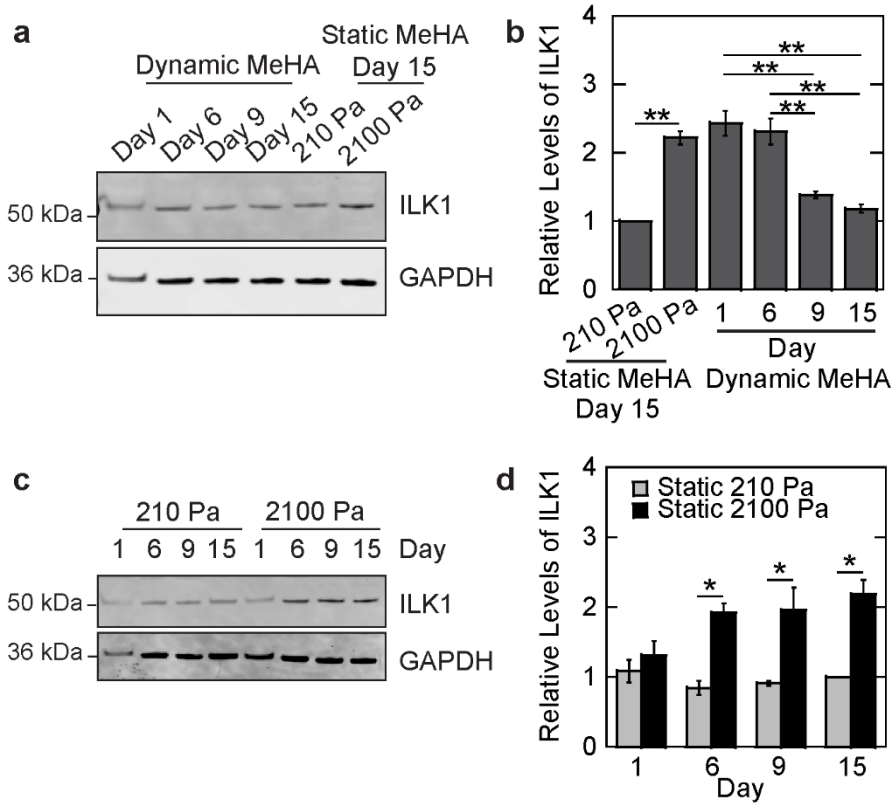

Figure 7. Dynamic softening of MeHA-based hydrogels decreases integrin-linked kinase (ILK1) expression in MDA-MB-231 breast cancer cells. a) Western blotting for ILK1 in MDA-MB-231 breast cancer cells seeded on static and dynamic MeHA-based hydrogels for various time-points. b) Densitometric analysis of ILK1 from blot shown in panel a. Data normalized with respect to static MeHA 210 Pa day 15 sample. Data indicate mean ± sem for n = 3 trials. **p<0.01. c) Western blotting for ILK1 in MDA-MB-231 breast cancer cells seeded on static MeHA-based hydrogels as a function of time. d) Densitometric analysis of ILK1 levels from blot shown in panel c. Data are normalized with respect to the static MeHA 210 Pa day 15 sample. Data indicate mean ± sem for n = 3 trials. *p<0.05, evaluated using analysis of variance (ANOVA) followed by Tukey's post-hoc test.

To examine whether ILK regulates phenotypic changes observed in cells as the dynamic hydrogel softens, MDA-MB-231 cells were treated with the ILK inhibitor QLT0267. When MDA-MB-231 cells are cultured on static 210 Pa hydrogels, treatment with QLT0267 does not have a significant effect on cell morphology or on the percentage of cells staining positive for Ki67 and cleaved caspase-3 in comparison to treatment with the vehicle control (**Figure S11a-d**). In contrast, when cells are cultured on the static 2100 Pa hydrogels treatment with QLT0267 leads to a reduction in cell spread area, cell aspect ratio, and the percentage of cells staining positive for Ki67 (**Figure S11e-g**). The percentage of cells staining positive for cleaved caspase-3 increases following QLT0267 treatment in comparison to treatment with the DMSO control, however, this difference was not statistically significant (**Figure S11h**). When cultured on dynamic hydrogels, at early time points (days 1-6) when the cells sense a 'stiff' matrix, treatment with QLT0267 promotes a decrease in cell spread area and aspect ratio, a decrease in the percentage of cells staining positive for Ki67, and an increase in the percentage of cells staining positive for cleaved caspase-3 in comparison to cells treated with the vehicle control (**Figure 8a-e**). On day 15 of culture on the dynamic hydrogels, when cells sense a 'soft' matrix, no differences are observed between the QLT0267 and control vehicle treated cells. Treatment with QLT0267 also impacts the expression of vimentin and E-cadherin in cells. Immunofluorescence staining reveals that MDA-MB-231 cells show low levels of vimentin when cultured on the static 2100 Pa and dynamic hydrogels and exhibit diffuse staining for E-cadherin after 15 days of culture with QLT0267 (**Figure 8f** and **Figure S12**). To confirm these findings, we also inhibited ILK signaling in MCF10A mammary epithelial cells. Treatment of MCF10A cells with QLT0267 promotes a decrease in vimentin in cells cultured on the static 2100 Pa and dynamic hydrogels, and an increase in E-cadherin expression and localization to cell-cell contacts in comparison to treatment with the vehicle control (**Figure 8g** and **Figure S13**). Together, these findings suggest that ILK plays an important role in regulating proliferation, cell survival, and protein expression as a function of matrix stiffness within this model system.

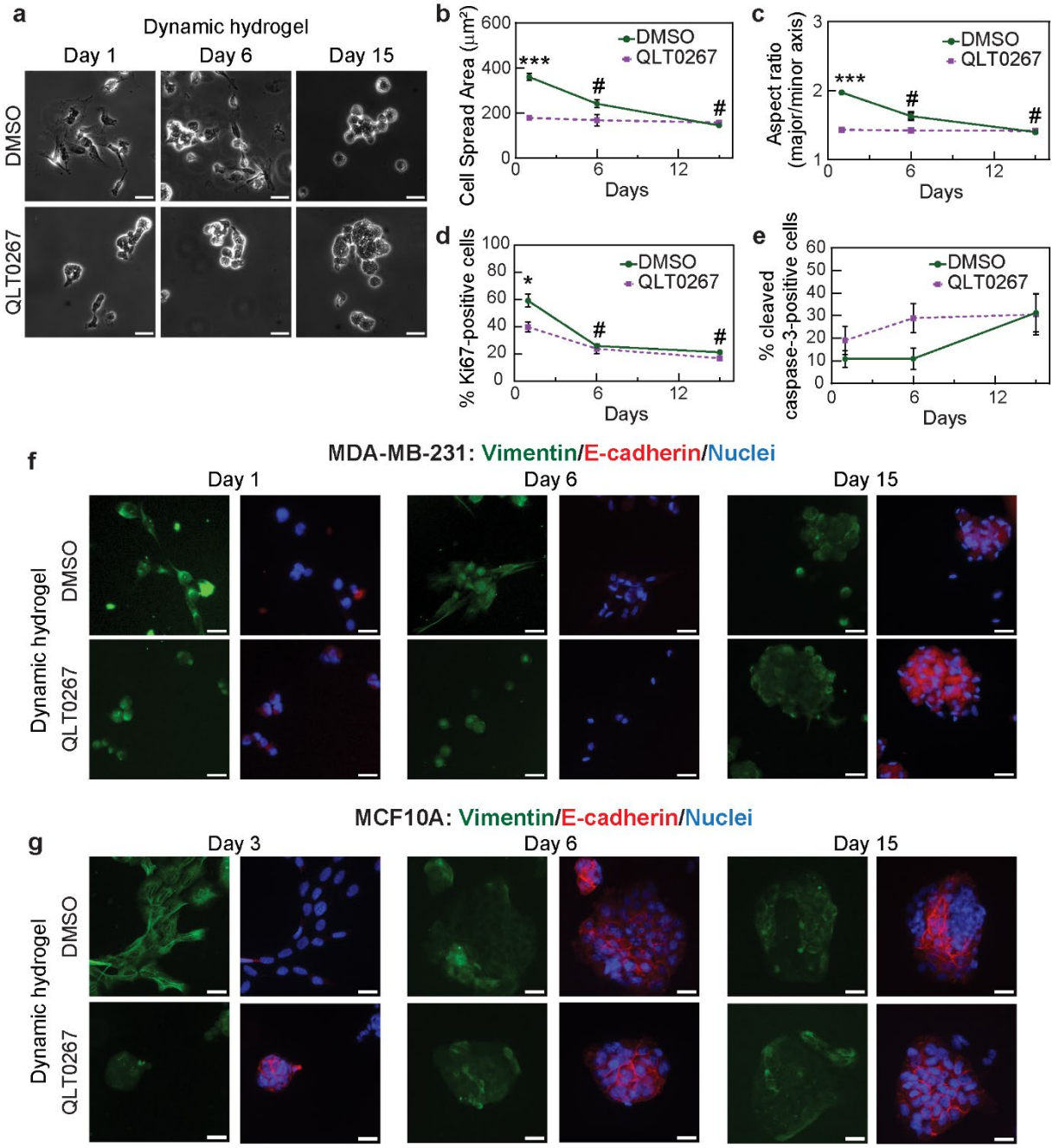

Figure 8. Inhibition of ILK activity impacts cell morphology, proliferation, survival, and protein expression in response to softening of MeHA hydrogels. a) Phase contrast microscopy images of MDA-MB-231 breast cancer cells cultured on dynamic MeHA-based hydrogels and treated with QLT0267 or DMSO vehicle control and monitored as a function of time. Scale bars: 25 μm. Quantification of b) cell spread area, c) cell aspect ratio, d) percentage of cells staining positive for Ki67, and e) percentage of cells staining positive for cleaved caspase-3 for MDA-MB-231 cells cultured on dynamic hydrogels and treated with QLT0267 or vehicle control. Data indicate mean ± sem for n = 3 trials. *$p<0.05$, ***$p<0.001$ in comparison to day 1 of QLT0267-treated sample, #$p<0.01$ for DMSO-treated samples in comparison to day 1 DMSO-treated sample, evaluated using analysis of variance (ANOVA) followed by Tukey's post-hoc test. Immunofluorescence staining for vimentin (green) and E-cadherin (red) for f) MDA-MB-231 breast cancer cells and g) MCF10A mammary epithelial cells cultured on dynamic hydrogels and treated with QLT0267 or vehicle control. Scale bars: 25 μm.

3. Discussion

Hydrogel platforms with tunable properties provide an approach to study cancer cell responses to microenvironmental cues. Previous studies have utilized MeHA-based platforms with a variety of chemical and photo-crosslinkers to tune the mechanical properties of the systems. For example, MeHA was crosslinked with Irgacure and UV light irradiation to mimic the modulus of normal mammary gland tissue (150 Pa), with further exposure to Irgacure and UV light promoting an increase in the hydrogel stiffness to mimic the mechanical properties of mammary tumors (3000 Pa).[17b] In a separate study, HA and gelatin were crosslinked using glycidyl methacrylate and magnetic microparticles were included to fabricate a 3D hydrogel network by a thiol-ene click reaction chemistry, and an applied magnetic field was used to reversibly tune the hydrogel stiffness from 560 Pa to 2640 Pa.[15] Furthermore, a 2D hyaluronic acid-poly-L-lysine hydrogel system was fabricated by including peptide sequences that are sensitive to matrix metalloproteinases (MMP) leading to dynamic softening of the hydrogel in response to MMPs secreted by breast cancer cells.[38] In this work, MeHA was crosslinked with Irgacure to create hydrogels with stable mechanical properties as a function of time. We also used the crosslinker PETMP in combination with Irgacure, as PETMP can undergo gradual hydrolysis with time, to create a hydrogel platform with tunable mechanical properties that mimic normal and diseased mammary tissue. This system builds upon previously developed dynamic hydrogel systems to develop a system with mechanical properties matched to the mammary gland. Moreover, the platform expands the repertoire of combinations of stable and degradable crosslinkers for use in tuning the mechanical properties of dynamic hydrogel systems. The amount of MeHA, composition and ratios of the crosslinkers, and parameters for light irradiation can be further tuned to create a hydrogel platform mimicking the mechanical properties of other healthy and diseased tissues beyond the mammary gland.

An increase in the stiffness of the matrix surrounding breast tumors is associated with cancer progression and these changes in stiffness can promote a mesenchymal phenotype in mammary epithelial cells and breast cancer cells. Indeed, MCF7 breast cancer cells exhibit a decrease in spheroid size, higher expression of vimentin, N-cadherin, SNAI1, SNAI2, Twist1, ZEB1, and lower expression of E-cadherin and ZO-1 with an increase in matrix stiffness from 560 Pa to 2640 Pa.[15] In another system, mammary epithelial cells exhibit a rounded morphology on soft 150 Pa hydrogels but transition to a spread morphology with loss of E-cadherin upon dynamic stiffening of the hydrogel to greater than 3000 Pa.[17b] These characteristic changes associated with induction of EMT in the cells were governed by TGFβ and transcription factors Twist1

and YAP.[17b] A similar trend was seen in cell clusters (PyMT cells derived from murine MMTV-PyMT tumors) cultured on alginate-matrigel based hydrogels with cells exhibiting enhanced protrusions, decreased circularity, decreased E-cadherin levels, elevation in N-cadherin, Twist, and Zeb1 levels, and increased migration as the stiffness gradually increased from 150 Pa to 1200 Pa.[39] Further, gradual stiffening of an alginate-based matrix has also been associated with increased resistance of MDA-MB-231 cells to doxorubicin as compared to cells cultured on soft substrates.[40] While these reports and others suggest that dynamic stiffening of the matrix promotes a mesenchymal phenotype in breast cancer cells, few studies have examined the impact of matrix mechanics on MET. In one such study, the effect of substrate softening from 576 kPa to 180 kPa on breast cancer cells was monitored, and it was found that matrix softening decreased the percentage of breast cancer cells exhibiting migratory properties as compared to cells cultured on stiff 491 kPa matrix.[38] However, the stiffnesses examined in the abovementioned study are outside physiologically relevant stiffnesses encountered by breast cancer cells *in vivo*. Together, our findings suggest that MCF10A mammary epithelial cells and MDA-MB-231 and MCF7 breast cancer cells exhibit mesenchymal-epithelial plasticity including a shift in morphology and gene expression as the matrix softens. As such, this platform holds promise for facilitating future studies examining mechanistic regulation of MET. While we examined the impact of matrix softening on breast cancer cells in this study, in the future the platform could be utilized to examine the impact of dynamic modulation of matrix stiffness on mesenchymal-epithelial plasticity in the context of other types of cancer.

The balance between cell proliferation and apoptosis coordinates development and tissue homeostasis, and disruption of these processes such as enhanced proliferation and/or impaired apoptosis can promote pathologies including cancer.[41] The mechanical properties of the cellular microenvironment can regulate both cell proliferation and apoptosis. An increase in matrix stiffness reduces apoptosis in cancer cells and shields them from immune cells and therapeutic drug treatments.[27] In hepatocellular carcinoma cells, an increase in matrix stiffness decreases the sensitivity of cells to the drug sorafenib and attenuates sorafenib-induced apoptosis in cancer cells.[42] Here, we find that when breast cancer cells are cultured on soft hydrogels, a higher percentage of cells stain positive for the apoptotic marker cleaved caspase-3 as compared to when the cells are cultured on stiff hydrogels with static mechanical properties. On the other hand, cell proliferation (observed via staining for Ki67) is higher in cells cultured on stiff hydrogels in comparison to on soft hydrogels. These results are consistent with previous

findings in breast cancer cells and in other cell types. Moreover, we build upon these findings and demonstrate a shift in proliferation and apoptosis in breast cancer cells as the matrix softens.

At secondary metastatic sites, it is thought that cancer cells exhibit MET to establish the secondary tumor. While cell proliferation is important for metastatic outgrowth, studies suggest that cancer cells can acquire a non-proliferative dormant phenotype and that tumors can also remain quiescent due to a balance between cell proliferation and death within the tumor.[43] Long-term relapse of cancer likely arises from activation of dormant cancer cells that reawaken and proliferate thereby promoting tumor outgrowth.[44] The factors regulating tumor cell dormancy are not well understood, but some studies suggest that soft microenvironments can promote a dormant phenotype in breast cancer cells.[45] Future efforts directed towards examining the impact of matrix mechanics on dormancy and evaluating how dynamic changes in matrix mechanics impact the activity of signaling molecules that regulate proliferation and apoptosis may provide further insight on regulatory mechanisms governing cancer and may help to identify new molecular targets to inhibit breast cancer cell proliferation and to promote cancer cell apoptosis.

Cells sense the mechanical properties of the extracellular matrix using cell surface integrins which promote activation of downstream signaling molecules including focal adhesion kinase and ILK.[36] ILK is particularly important as it has been shown to mediate apoptosis, proliferation, and gene expression in breast cancer cells and other cell types[36-37, 46] and evidence supports that ILK signaling is regulated by mechanical cues.[37, 46c, 47] Indeed, ILK regulates a stiffness-induced switch between EMT and apoptosis in normal mammary gland epithelial cells.[37] Knockdown of ILK attenuates Twist-induced EMT in human MCF10A mammary epithelial cells and promotes an increase in E-cadherin expression and decrease in vimentin, fibronectin and N-cadherin.[48] Overexpression of ILK can enhance the expression of vimentin, snail and slug and decrease the expression of E-cadherin in colorectal cancer cells.[49] Furthermore, knockdown of ILK in MDA-MB-231 cancer cells results in a decrease in cell proliferation while overexpression of ILK in MCF7 cells enhances cell growth and viability via activation of the PI3K/Akt pathway.[46b] Interestingly, an increase in matrix stiffness from 130 Pa to 4020 Pa along with hypoxic conditions has been shown to promote an increase in the levels of ILK in MDA-MB-231 breast cancer cells.[46c] On the other hand, another study showed that ILK expression is higher in MDA-MB-231 cells when cultured on 38 kPa hydrogels in comparison to when cultured on 10 kPa or 57 kPa hydrogels.[47a] Here, we find that MDA-MB-

231 breast cancer cells express higher levels of ILK1 protein when cultured on 2100 Pa hydrogels in comparison to when cultured on 210 Pa hydrogels with static mechanical properties. Discrepancies between these studies and previous reports could be attributed to differences in the magnitude of matrix stiffness utilized in the various systems. Nonetheless, the decrease in ILK1 levels that we observe correlates with a decrease in proliferation and expression of mesenchymal markers and an increase in apoptosis and expression of epithelial markers. We find that pharmacological inhibition of ILK activity attenuates cell proliferation, increases apoptosis, and reduces the expression of vimentin in MDA-MB-231 and MCF10A cells cultured on stiff matrices. Together, these findings suggest that these cell fates are controlled by a mechanotransduction cascade involving ILK. Future studies focused on how matrix stiffness regulates ILK expression may provide further mechanistic insight into how mechanical signals impact cancer cell fate decisions.

Our findings suggest that targeting the stiffness of the extracellular matrix can potentially be used as a therapeutic approach to slow the progression of cancer, namely by providing a microenvironment with mechanical properties conducive to maintaining an epithelial phenotype in cancer cells. Indeed, targeting the extracellular matrix can improve the efficiency of therapeutic cancer drugs. For example, treatment with losartan leads to a decrease in collagen I synthesis by cancer-associated fibroblasts that are isolated from biopsies of breast cancer patients, which promotes a reduction in stromal collagen and an improvement in the efficacy of liposomal doxorubicin.[50] Furthermore, the Rho kinase (ROCK) inhibitor Fasudil reduces fibroblast contraction, decreases matrix stiffness, improves the response of pancreatic cancer cells to therapeutics, and decreases cancer cell invasion.[51] Further *in vivo* studies examining the impact of a reduction in matrix stiffness within the tumor microenvironment on the characteristics of diverse types of cancer cells are warranted and may suggest novel approaches for reducing the progression of cancer.

4. Conclusion

We describe a dynamic HA-based hydrogel for examination of mesenchymal-epithelial plasticity in breast cancer cells. In contrast to hydrogels with static mechanical properties, our platform enables observation of the dynamics of cell transitions and reveals intermediate epithelial/mesenchymal states as mammary cells progress through a stiffness mediated MET trajectory. Gradual softening of the hydrogel promotes temporal changes in breast cancer cell morphology, actin organization, and gene expression and these changes are consistent with a

transition from a mesenchymal to an epithelial phenotype. In addition, a dynamic reduction in matrix stiffness promotes apoptosis and attenuates proliferation in MDA-MB-231 breast cancer cells. Furthermore, we find that a dynamic reduction in stiffness leads to a reduction in ILK expression. Inhibition of ILK blocks matrix stiffness induced cell proliferation and expression of mesenchymal markers. Together, these observations demonstrate an important role for matrix mechanics in regulating MET-associated changes in breast cancer cells.

5. Experimental Section/Methods

Synthesis of MeHA macromer: Methacrylated hyaluronic acid (MeHA) was synthesized following published protocols.[52] Sodium hyaluronate with nominal molecular weight of 73 kDa (Lifecore Biomedical) was dissolved in deionized (DI) water at 1 w/v% concentration and reacted with 6-fold molar excess of methacrylate anhydride at pH 8. The reaction was performed in a jacketed reactor and the temperature was maintained at 4 °C with continuous stirring. A pH of 8 was maintained by frequent pH monitoring and adding a 5 M solution of potassium hydroxide in DI water dropwise along with continuous stirring for 6 to 8 hours. The reaction was then allowed to run overnight at 4 °C. The reaction mixture was precipitated with cold acetone at a 5:1 volumetric ratio and the precipitate was recovered using vacuum filtration and centrifugation at 9000 rpm. The precipitate was then re-dissolved in DI water. The solution was dialyzed in 6-8 kDa tubing against DI water at 4 °C for three days, with the bath water changed out twice daily. The MeHA solution was then lyophilized by freeze-drying for another 3 days using a Labconco Freezone 2.5 operated at -50 °C. A sample of the MeHA was dissolved in deuterated water and the degree of methacrylate functionalization was analyzed using Hydrogen Nuclear Magnetic Resonance (^{1}H NMR) on a Bruker NEO-400 instrument in the NMR Facility at Penn State. The peaks at a chemical shift of 6 ppm, representing the methacrylate group, were normalized by peaks between a chemical shift of 3 and 4 ppm, representing the native HA backbone, to determine the degree of methacrylation of MeHA. The ^{1}H NMR data are shown in Figure S1. The methacrylate functionalization of MeHA was determined to be 39%.

MeHA hydrogel fabrication: MeHA stock solution was prepared by dissolving MeHA at 4 w/v% in 1× phosphate buffered saline (PBS) containing 0.2 M triethanolamine. Irgacure was dissolved at 1 w/v% in ethanol. For fabrication of static hydrogels, the hydrogel solution was formulated by mixing MeHA with Irgacure with a final concentration of MeHA of 2 w/v% and Irgacure of 0.05 w/v%. For fabrication of dynamic hydrogels, pentaerythritol tetrakis(3-

mercaptopropionate) (PETMP) was dissolved in acetone and a mole ratio of 0.006 PETMP:MeHA was used. The hydrogel solution was pipetted onto the surface of 2-aminopropyltrimethoxysilane (APTMS) and glutaraldehyde-treated 22-mm square glass coverslips. A 22-mm diameter RAIN-X treated circular coverslip was then placed on top of the solution. The hydrogels were then placed in a UVP CL-1000 Ultraviolet Crosslinker (302 nm) for the indicated times for static hydrogels and for 15 sec for dynamic hydrogels to initiate Irgacure crosslinking of MeHA. To prepare the dynamic hydrogels, the samples were then incubated for an additional 3 hours at room temperature to allow PETMP to react with the MeHA. The dynamic hydrogels were then rinsed with 1× PBS 5 times and kept in fresh PBS solution overnight on a shaker at 37 °C to remove residual PETMP. After overnight shaking, the PBS was aspirated and the hydrogels were transferred to either a fresh 1× PBS solution (for hydrogel characterization and stored at 37 °C with periodic PBS solution changes every 3 days) or activated for fibronectin attachment.

MeHA hydrogel characterization: Hydrogel moduli were characterized using a Bruker Bioscope Resolve Bio-atomic force microscope (AFM) placed on a Nikon TE2000 inverted microscope at the Materials Characterization Lab at Penn State. MLCT probes (Bruker) with a silicon nitride cantilever C having a nominal tip radius of 20 nm, half-angle of 17.5° and spring constant of 0.01 N/m were utilized for mechanical characterization. All of the AFM characterization experiments were performed in 1× PBS (fluid conditions) and at room temperature. The Peak Force Quantitative NanoMechanics (QNM) in fluid (Bruker) software package was utilized for data acquisition and analysis. Prior to hydrogel characterization, the MLCT probe was mounted and allowed to stabilize under fluid conditions. Before every characterization experiment, the probe was calibrated by allowing it to engage on a clean glass slide, i.e., a hard sample, kept in 1× PBS solution to evaluate the calibrated spring constant and the deflection sensitivity of the probe. The revised values for the spring constant were then inputted to the software along with setting the Poisson ratio as 0.5 as reported by others.[53]

The hydrogel samples were rinsed twice with 1× PBS to remove debris or dust particles prior to engaging the AFM probe. All measurements were performed with a ramp size of 5 μm and a frequency of 1 Hz. A scan size of 500 nm in X and Y was used and the lateral resolution was fixed at 16 × 16. A total of 256 force curves were obtained per scan. Because of the tip geometry, Young's moduli were determined using the Sneddon model for every 256 grid by the NanoScope Analysis 2.0 software (Bruker). The average of all the grid moduli values was

evaluated to compute the Young's modulus for the 500 nm × 500 nm scan. For every trial, AFM measurements were performed on at least three different regions per hydrogel sample and the Young's modulus of the hydrogel sample for that trial was computed by averaging the Young's moduli of all the individual scans.

Cell culture: The human breast cancer cell lines MDA-MB-231 (HTB-26) and MCF7 (HTB-22) and human mammary epithelial cell line MCF10A (CRL-10317) were purchased from the American Type Culture Collection (ATCC). The cells were grown according to the recommendations of ATCC. MDA-MB-231 cells were maintained in Dulbecco's Modified Eagle Medium (DMEM; Corning) with 10% (v/v) fetal bovine serum (FBS; Atlanta Biologicals) and 50 μg/ml gentamicin (Gibco). MCF7 cells were grown in Eagle's Minimum Essential Medium (EMEM; ATCC) with 10% (v/v) FBS, 50 μg/ml gentamicin, and 10 μg/ml insulin (Sigma Aldrich). MCF10A cells were grown in DMEM/F12 media (Fisher) with 5% horse serum (Fisher), 20 ng/mL hEGF (Thermo), 0.5 μg/mL hydrocortisone (Sigma), 100 ng/mL Cholera toxin (Sigma), 10 μg/mL insulin (Sigma Aldrich), and 10 U/mL Pen/Strep (VWR). Upon seeding to hydrogels, MCF10A cell media was replaced with low serum media (2% horse serum and 5 ng/mL hEGF). Media was changed every 2-3 days. Cells were cultured at 37 °C in a humidified 5% CO_2 environment. QLT0267 (Sigma) was diluted in DMSO and added at a concentration of 10 μM to cells 24 hours after plating the cells to the hydrogels. For inhibitor studies the time point day 1 is 24 hours after QLT0267 treatment.

Hydrogel activation and cell seeding: Functionalization of MeHA hydrogels with matrix proteins occurred 24 hours after hydrogel synthesis. Hydrogel surfaces were activated using 20 mM 1-ethyl-3-(3-dimethylaminopropyl) carbodiimide hydrochloride (EDC) and 50 mM N-hydroxysuccinimide (NHS; Thermo Scientific) prepared in MES buffer solution (0.1 M 2-(N-Morpholino) ethanesulfonic acid hydrate (MES hydrate; Sigma) and 0.5 M NaCl dissolved in water). Hydrogels were incubated with a 25 μg/ml solution of human plasma fibronectin (Gibco) for 4-5 hours at 37 °C. The hydrogels were then thoroughly rinsed with 1× PBS and cells were seeded at 40000 cells/cm^2 to the hydrogels. For collagen coating, rat tail type I collagen (Advanced BioMatrix) was diluted to 100 μg/mL in 0.1% acetic acid solution and hydrogels were incubated with the collagen solution for 2 hours at room temperature. The hydrogels were then thoroughly rinsed with 1× PBS and cells were seeded at 40000 cells/cm^2 to the hydrogels. Day 1 of experiments is 24 hours after seeding cells to the hydrogels.

Western blotting: For whole-cell protein extractions, cells on MeHA hydrogels were lysed using ice-cold RIPA buffer containing Halt protease and phosphatase inhibitors (Thermo Scientific). The total protein concentration was quantified using a Pierce BCA Protein Assay Kit (Thermo Scientific) or a Bradford assay using Coomassie Plus Assay Reagent (Thermo Scientific). For gel electrophoresis, protein samples were denatured using NuPAGE LDS sample buffer (Invitrogen) and NuPAGE sample reducing agent (Invitrogen) at 70 ºC for 10 min. Equal amounts of protein were loaded and were separated on a NuPAGE 4-12% bis-tris gel (Invitrogen) using NuPAGE (2-(N-morpholino) ethanesulfonic acid) MES Sodium dodecyl sulfate (SDS) running buffer (Invitrogen) in a XCell SureLock Cell powered by a Bio-Rad PowerPac HC. Proteins were transferred to a nitrocellulose or PVDF membrane using a XCell II Blot Module. The membrane was then blocked in a solution of 5% w/v non-fat dry milk or 5% w/v BSA in 1× Tris-buffered saline plus 0.1% Tween (TBST). The membranes were probed with primary antibodies overnight at 4 ºC. Primary antibodies include: E-cadherin (1:1000; 24E10 Cell Signaling), vimentin (1:1000; V5255, Sigma Aldrich), pan-cytokeratin (1:1000; C2562, Sigma Aldrich), fibronectin (1:1000; F3648, Sigma Aldrich), Snail (1:750; L70G2, Cell Signaling), and ILK1 (1:1000; 3862S, Cell Signaling). Membranes were then washed three times with 1× TBST buffer and incubated with IRDye secondary antibodies (1:15000; IRDye 680 RD and 1:15000; IRDye 800 CW, LI-COR Biosciences) at room temperature for 1 hour and then washed again three times with 1× TBST. Western blots were imaged using a LI-COR Odyssey Infrared imaging system.

Densitometric analysis of blot images was performed using ImageJ software. For each protein sample, the normalized intensity was obtained by dividing the intensity of the target protein by the intensity of the loading control. Relative levels or fold changes between samples were evaluated by dividing the normalized intensity of the samples by that of the control sample for that set of experiments.

Immunofluorescence staining: For staining of E-cadherin, cleaved caspase-3, and Ki67, breast cancer cells cultured on MeHA hydrogels were rinsed with 1× PBS and fixed in 4% paraformaldehyde at room temperature for 15 min. After fixation, samples were treated with 0.5% v/v IGEPAL (Sigma) and twice permeabilized with 0.1% v/v Triton X-100 each for 10 min. For staining of vimentin, cells were fixed with 1:1 methanol:acetone and permeabilized with 0.1% v/v Triton X-100 for 10 min. Samples were then blocked with 5% goat serum (Sigma Aldrich) or 5% bovine serum albumin (BSA; Sigma Aldrich) in 1× PBS for 1 hour and

incubated with primary antibodies to vimentin (1:200; V5255, Sigma Aldrich), E-cadherin (1:200; 24E10, Cell Signaling), cleaved caspase-3 (1:400; Asp175, 9661S, Cell Signaling) or Ki67 (1:250; SP6, ab16667, Abcam) overnight at 4 ºC. For co-staining of E-cadherin and vimentin, cells were fixed with 50:50 methanol:acetone for 10 minutes at -20 °C, permeabilized with 0.1% Triton X-100 for 10 minutes at room temperature, blocked with 5% BSA in 1× PBS for 2 hours, then incubated overnight at 4 °C with primary antibodies for E-cadherin (1:200, 24E10, Cell Signaling) and vimentin (1:200, V5255, Sigma Aldrich). For co-staining of cleaved caspase-3 and Ki67, cells were fixed with 4% paraformaldehyde for 15 minutes at room temperature, permeabilized with 0.1% Triton X-100 for 10 minutes at room temperature, blocked with 5% goat serum and 0.3% Triton X-100 in 1× PBS for 2 hours, then incubated overnight at 4 °C with primary antibodies for cleaved caspase-3 (1:400, Asp175, 9661S, Cell Signaling) and Ki67 (1:1600, 8D5, 9449, Cell Signaling). Samples were rinsed in 1× PBS three times to remove unbound primary antibody before incubating with Alexa Fluor secondary antibodies (1:500; Alexa Fluor 594 goat anti-rabbit (Invitrogen A-11037) and Alexa Fluor 488 goat anti-mouse (Invitrogen A-11029)) at room temperature for 1 hour. Samples were then rinsed with 1× PBS three times to remove unbound secondary antibody. For F-actin staining, cells cultured on MeHA hydrogels were rinsed with 1× PBS and fixed in 4% paraformaldehyde at room temperature for 15 min, permeabilized with 0.1% Triton X-100 for 5 min at room temperature and blocked in 1% BSA in 1× PBS for 25 min. Cells were incubated with Alexa Fluor 594 phalloidin (1:150; Invitrogen) or with fluorescent dye 488-I phalloidin (1:1000; U0281, Abnova) for 25 min or 45 min respectively at room temperature and rinsed with 1× PBS three times to remove unbound phalloidin. Nuclei of cells were counterstained with Hoechst 33342 (Life Technologies) before mounting the samples on slides using Fluoromount-G (Invitrogen).

Microscopy and image analysis: Stained samples were imaged using a 20× or 40× objective on a Nikon Eclipse Ti-E inverted fluorescence microscope equipped with a Photometrics CoolSNAP HQ2 charged-coupled device (CCD) camera. Imaging conditions and settings were kept constant for all sample treatments. ImageJ was used to compute the cell spread area and aspect ratio using the 'shape descriptors' measurement tool after outlining the cell boundary from phase contrast microscopy images. For evaluating the percentage cells expressing cleaved caspase-3 and Ki67, the number of cells staining positive for cleaved caspase-3 and Ki67 was divided by the total number of cells within the analyzed images.

Statistical analysis: Data are reported as mean ± standard error of the mean. All experiments including hydrogel characterization were repeated three times, unless otherwise noted. To facilitate comparison of protein levels between samples, normalization to control samples was performed and is indicated in the respective figure captions. For normally distributed data, an analysis of variance (ANOVA) followed by Tukey's post-hoc test for comparing means of multiple samples was performed using Minitab or GraphPad Prism version 9.5.1 for sample comparison. Differences were considered significant for p-values less than 0.05 and are indicated as *$p<0.05$, **$p<0.01$ and ***$p<0.001$ within figures.

Supporting Information

Supporting Information is available from the Wiley Online Library or from the author.

Data availability statement

The data that support the findings of this study are available from the corresponding author upon reasonable request.

Conflict of interest disclosure

The authors declare no competing interests

Acknowledgements

This work was supported by the National Science Foundation (CMMI-1751785). The authors would like to acknowledge Dr. Timothy Tighe, Dr. Sarah Kiemle, and Dr. Markus Kastner at the Penn State Materials Characterization Lab for help with Bruker BioResolve AFM characterization measurements. The authors would also like to thank Dr. Justin Brown (Penn State) for use of the LI-COR Odyssey Imaging System for imaging western blots and Dr. Andrew Zydney (Penn State) for use of plate readers for protein analysis.

C.S. Sankhe, J.L. Sacco, E.D. Gomez, and E.W. Gomez conceptualized and designed the experiments. R. Fair, M.K.R. Aldahdooh, and J. Lawton synthesized the MeHA and characterized the synthesis products. C.S. Sankhe, J.L. Sacco, and D.V.R. Soares performed the experiments. C.S. Sankhe and E.W. Gomez wrote the original draft of the manuscript. All authors contributed to data analysis and provided comments regarding the manuscript.

Received: ((will be filled in by the editorial staff))
Revised: ((will be filled in by the editorial staff))
Published online: ((will be filled in by the editorial staff))

References

[1] a)C. L. Chaffer, E. W. Thompson, E. D. Williams, *Cells Tissues Organs* **2007**, 185, 7; b)H. Y. Kim, T. R. Jackson, L. A. Davidson, *Semin Cell Dev Biol* **2016**.

[2] a)N. P. Gunasinghe, A. Wells, E. W. Thompson, H. J. Hugo, *Cancer Metastasis Rev* **2012**, 31, 469; b)D. Yao, C. Dai, S. Peng, *Mol Cancer Res* **2011**, 9, 1608; c)C. Scheel, R. A. Weinberg, *Semin Cancer Biol* **2012**, 22, 396; d)U. Jeschke, I. Mylonas, C. Kuhn, N. Shabani, C. Kunert-Keil, C. Schindlbeck, B. Gerber, K. Friese, *Anticancer Res* **2007**, 27, 1969; e)M. Korpal, B. J. Ell, F. M. Buffa, T. Ibrahim, M. A. Blanco, T. Celia-Terrassa, L. Mercatali, Z. Khan, H. Goodarzi, Y. Hua, Y. Wei, G. Hu, B. A. Garcia, J. Ragoussis, D. Amadori, A. L. Harris, Y. Kang, *Nat Med* **2011**, 17, 1101; f)D. Park, R. Karesen, U. Axcrona, T. Noren, T. Sauer, *APMIS* **2007**, 115, 52; g)P. Samavarchi-Tehrani, A. Golipour, L. David, H. K. Sung, T. A. Beyer, A. Datti, K. Woltjen, A. Nagy, J. L. Wrana, *Cell Stem Cell* **2010**, 7, 64; h)R. Li, J. Liang, S. Ni, T. Zhou, X. Qing, H. Li, W. He, J. Chen, F. Li, Q. Zhuang, B. Qin, J. Xu, W. Li, J. Yang, Y. Gan, D. Qin, S. Feng, H. Song, D. Yang, B. Zhang, L. Zeng, L. Lai, M. A. Esteban, D. Pei, *Cell Stem Cell* **2010**, 7, 51; i)C. L. Chaffer, J. P. Brennan, J. L. Slavin, T. Blick, E. W. Thompson, E. D. Williams, *Cancer Res* **2006**, 66, 11271.

[3] a)Y. L. Chao, C. R. Shepard, A. Wells, *Mol Cancer* **2010**, 9, 179; b)C. C. Yates, C. R. Shepard, D. B. Stolz, A. Wells, *Br J Cancer* **2007**, 96, 1246; c)D. Pei, X. Shu, A. Gassama-Diagne, J. P. Thiery, *Nature Cell Biology* **2019**, 21, 44.

[4] a)M. von Dassow, L. A. Davidson, *Dev Dyn* **2009**, 238, 2; b)J. Zhou, H. Y. Kim, J. H. Wang, L. A. Davidson, *Development* **2010**, 137, 2785; c)T. R. Jackson, H. Y. Kim, U. L. Balakrishnan, C. Stuckenholz, L. A. Davidson, *Curr Biol* **2017**, 27, 1326.

[5] B. Hinz, *J Biomech* **2010**, 43, 146.

[6] a)M. J. Paszek, N. Zahir, K. R. Johnson, J. N. Lakins, G. I. Rozenberg, A. Gefen, C. A. Reinhart-King, S. S. Margulies, M. Dembo, D. Boettiger, D. A. Hammer, V. M. Weaver, *Cancer Cell* **2005**, 8, 241; b)J. I. Lopez, I. Kang, W.-K. You, D. M. McDonald, V. M. Weaver, *Integrative biology : quantitative biosciences from nano to macro* **2011**, 3, 910.

[7] a)E. W. Gomez, Q. K. Chen, N. Gjorevski, C. M. Nelson, *J Cell Biochem* **2010**, 110, 44; b)J. W. O'Connor, E. W. Gomez, *PLoS One* **2013**, 8, e83188; c)J. W. O'Connor, K. Mistry, D. Detweiler, C. Wang, E. W. Gomez, *Sci Rep* **2016**, 6, 26226.

[8] a)A. C. Brown, V. F. Fiore, T. A. Sulchek, T. H. Barker, *J Pathol* **2013**, 229, 25; b)J. L. Leight, M. A. Wozniak, S. Chen, M. L. Lynch, C. S. Chen, *Mol Biol Cell* **2012**, 23, 781; c)J. W. O'Connor, P. N. Riley, S. M. Nalluri, P. K. Ashar, E. W. Gomez, *J Cell Physiol* **2015**,

230, 1829; d)S. C. Wei, L. Fattet, J. H. Tsai, Y. Guo, V. H. Pai, H. E. Majeski, A. C. Chen, R. L. Sah, S. S. Taylor, A. J. Engler, J. Yang, *Nat Cell Biol* **2015**, 17, 678.

[9] R. L. Heise, V. Stober, C. Cheluvaraju, J. W. Hollingsworth, S. Garantziotis, *J Biol Chem* **2011**, 286, 17435.

[10] a)M. M. Giacomini, M. A. Travis, M. Kudo, D. Sheppard, *Exp Cell Res* **2012**, 318, 716; b)J. S. Munger, X. Huang, H. Kawakatsu, M. J. Griffiths, S. L. Dalton, J. Wu, J. F. Pittet, N. Kaminski, C. Garat, M. A. Matthay, D. B. Rifkin, D. Sheppard, *Cell* **1999**, 96, 319.

[11] a)J. P. Thiery, H. Acloque, R. Y. Huang, M. A. Nieto, *Cell* **2009**, 139, 871; b)X. Liu, H. Sun, J. Qi, L. Wang, S. He, J. Liu, C. Feng, C. Chen, W. Li, Y. Guo, D. Qin, G. Pan, J. Chen, D. Pei, H. Zheng, *Nat Cell Biol* **2013**, 15, 829.

[12] a)J. Haerinck, S. Goossens, G. Berx, *Nat Rev Genet* **2023**, 24, 590; b)T. Celia-Terrassa, C. Bastian, D. D. Liu, B. Ell, N. M. Aiello, Y. Wei, J. Zamalloa, A. M. Blanco, X. Hang, D. Kunisky, W. Li, E. D. Williams, H. Rabitz, Y. Kang, *Nat Commun* **2018**, 9, 5005.

[13] a)J. T. Thaiparambil, L. Bender, T. Ganesh, E. Kline, P. Patel, Y. Liu, M. Tighiouart, P. M. Vertino, R. D. Harvey, A. Garcia, A. I. Marcus, *Int J Cancer* **2011**, 129, 2744; b)D. R. Pattabiraman, B. Bierie, K. I. Kober, P. Thiru, J. A. Krall, C. Zill, F. Reinhardt, W. L. Tam, R. A. Weinberg, *Science* **2016**, 351, aad3680; c)Y. B. Lin G, Liang Z, Li L, Qu S, Chen K, Zhou L, Lu Q, Sun Y, Zhu X., *Onco Targets Ther.* **2018**, 3805; d)M. Shen, Z. Xu, W. Xu, K. Jiang, F. Zhang, Q. Ding, Z. Xu, Y. Chen, *Journal of Experimental & Clinical Cancer Research* **2019**, 38, 149.

[14] A. J. Rice, E. Cortes, D. Lachowski, B. C. H. Cheung, S. A. Karim, J. P. Morton, A. Del Río Hernández, *Oncogenesis* **2017**, 6, e352.

[15] Y. Shou, X. Y. Teo, X. Li, L. Zhicheng, L. Liu, X. Sun, W. Jonhson, J. Ding, C. T. Lim, A. Tay, *ACS Nano* **2023**, 17, 2851.

[16] a)R. S. Stowers, S. C. Allen, L. J. Suggs, *Proceedings of the National Academy of Sciences* **2015**, 112, 1953; b)K. Homma, A. C. Chang, S. Yamamoto, R. Tamate, T. Ueki, J. Nakanishi, *Acta Biomaterialia* **2021**, 132, 103; c)I. N. Lee, O. Dobre, D. Richards, C. Ballestrem, J. M. Curran, J. A. Hunt, S. M. Richardson, J. Swift, L. S. Wong, *ACS Applied Materials & Interfaces* **2018**, 10, 7765; d)C. Yang, M. W. Tibbitt, L. Basta, K. S. Anseth, *Nature Materials* **2014**, 13, 645; e)S. R. Caliari, M. Perepelyuk, B. D. Cosgrove, S. J. Tsai, G. Y. Lee, R. L. Mauck, R. G. Wells, J. A. Burdick, *Scientific Reports* **2016**, 6, 21387.

[17] a)M. G. Ondeck, A. J. Engler, *Journal of Biomechanical Engineering* **2016**, 138; b)M. G. Ondeck, A. Kumar, J. K. Placone, C. M. Plunkett, B. F. Matte, K. C. Wong, L. Fattet, J. Yang, A. J. Engler, *Proceedings of the National Academy of Sciences* **2019**, 116, 3502.

[18] S. R. Caliari, M. Perepelyuk, E. M. Soulas, G. Y. Lee, R. G. Wells, J. A. Burdick, *Integrative Biology* **2016**, 8, 720.

[19] a)M. de la Torre, A. F. Wells, J. Bergh, A. Lindgren, *Hum Pathol* **1993**, 24, 1294; b)P. Auvinen, R. Tammi, J. Parkkinen, M. Tammi, U. Agren, R. Johansson, P. Hirvikoski, M. Eskelinen, V. M. Kosma, *Am J Pathol* **2000**, 156, 529.

[20] A. Zoltan-Jones, L. Huang, S. Ghatak, B. P. Toole, *J Biol Chem* **2003**, 278, 45801.

[21] M. Plodinec, M. Loparic, C. A. Monnier, E. C. Obermann, R. Zanetti-Dallenbach, P. Oertle, J. T. Hyotyla, U. Aebi, M. Bentires-Alj, R. Y. H. Lim, C.-A. Schoenenberger, *Nature Nanotechnology* **2012**, 7, 757.

[22] a)G. K. Koukoulis, A. A. Howeedy, M. Korhonen, I. Virtanen, V. E. Gould, *J Submicrosc Cytol Pathol* **1993**, 25, 285; b)E. Ioachim, A. Charchanti, E. Briasoulis, V. Karavasilis, H. Tsanou, D. L. Arvanitis, N. J. Agnantis, N. Pavlidis, *Eur J Cancer* **2002**, 38, 2362; c)L. Christensen, *APMIS Suppl* **1992**, 26, 1.

[23] a)C. L. Li, D. Yang, X. Cao, F. Wang, D. Y. Hong, J. Wang, X. C. Shen, Y. Chen, *Oncol Lett* **2017**, 13, 3889; b)J. Park, J. E. Schwarzbauer, *Oncogene* **2014**, 33, 1649.

[24] a)O. Maller, A. P. Drain, A. S. Barrett, S. Borgquist, B. Ruffell, I. Zakharevich, T. T. Pham, T. Gruosso, H. Kuasne, J. N. Lakins, I. Acerbi, J. M. Barnes, T. Nemkov, A. Chauhan, J. Gruenberg, A. Nasir, O. Bjarnadottir, Z. Werb, P. Kabos, Y. Y. Chen, E. S. Hwang, M. Park, L. M. Coussens, A. C. Nelson, K. C. Hansen, V. M. Weaver, *Nat Mater* **2021**, 20, 548; b)C. W. Huo, G. Chew, P. Hill, D. Huang, W. Ingman, L. Hodson, K. A. Brown, A. Magenau, A. H. Allam, E. McGhee, P. Timpson, M. A. Henderson, E. W. Thompson, K. Britt, *Breast Cancer Res* **2015**, 17, 79; c)P. P. Provenzano, D. R. Inman, K. W. Eliceiri, J. G. Knittel, L. Yan, C. T. Rueden, J. G. White, P. J. Keely, *BMC Med* **2008**, 6, 11.

[25] a)G. Carmona, U. Perera, C. Gillett, A. Naba, A. L. Law, V. P. Sharma, J. Wang, J. Wyckoff, M. Balsamo, F. Mosis, M. De Piano, J. Monypenny, N. Woodman, R. E. McConnell, G. Mouneimne, M. Van Hemelrijck, Y. Cao, J. Condeelis, R. O. Hynes, F. B. Gertler, M. Krause, *Oncogene* **2016**, 35, 5155; b)G. Jacquemet, I. Paatero, A. F. Carisey, A. Padzik, J. S. Orange, H. Hamidi, J. Ivaska, *Journal of Cell Biology* **2017**, 216, 3387; c)L. M. Machesky, *FEBS Letters* **2008**, 582, 2102.

[26] S. M. Nalluri, J. W. O'Connor, E. W. Gomez, *Cytoskeleton (Hoboken)* **2015**, 72, 557.

[27] a)B. Yao, Y. Niu, Y. Li, T. Chen, X. Wei, Q. Liu, *J Cancer* **2020**, 11, 6188; b)Y. Shen, X. Wang, J. Lu, M. Salfenmoser, N. M. Wirsik, N. Schleussner, A. Imle, A. Freire Valls, P. Radhakrishnan, J. Liang, G. Wang, T. Muley, M. Schneider, C. Ruiz de Almodovar, A. Diz-Muñoz, T. Schmidt, *Cancer Cell* **2020**, 37, 800.

[28] A. Hollestelle, J. K. Peeters, M. Smid, M. Timmermans, L. C. Verhoog, P. J. Westenend, A. A. J. Heine, A. Chan, A. M. Sieuwerts, E. A. C. Wiemer, J. G. M. Klijn, P. J. van der Spek, J. A. Foekens, M. Schutte, M. A. den Bakker, J. W. M. Martens, *Breast Cancer Research and Treatment* **2013**, 138, 47.

[29] J. R. Graff, J. G. Herman, R. G. Lapidus, H. Chopra, R. Xu, D. F. Jarrard, W. B. Isaacs, P. M. Pitha, N. E. Davidson, S. B. Baylin, *Cancer Res* **1995**, 55, 5195.

[30] C. Dong, Y. Wu, Y. Wang, C. Wang, T. Kang, P. G. Rychahou, Y. I. Chi, B. M. Evers, B. P. Zhou, *Oncogene* **2013**, 32, 1351.

[31] a)H. Eslami Amirabadi, M. Tuerlings, A. Hollestelle, S. SahebAli, R. Luttge, C. C. van Donkelaar, J. W. M. Martens, J. M. J. den Toonder, *Biomedical Microdevices* **2019**, 21, 101; b)R. B. Hazan, G. R. Phillips, R. F. Qiao, L. Norton, S. A. Aaronson, *J Cell Biol* **2000**, 148, 779.

[32] a)S. Sivagurunathan, A. Vahabikashi, H. Yang, J. Zhang, K. Vazquez, D. Rajasundaram, Y. Politanska, H. Abdala-Valencia, J. Notbohm, M. Guo, S. A. Adam, R. D. Goldman, *Front Cell Dev Biol* **2022**, 10, 929495; b)H. Polioudaki, S. Agelaki, R. Chiotaki, E. Politaki, D. Mavroudis, A. Matikas, V. Georgoulias, P. A. Theodoropoulos, *BMC Cancer* **2015**, 15, 399.

[33] a)X. Li, J. Yao, X. Yang, W. Tian, L. Liu, *Applied Surface Science* **2008**, 255, 459; b)K. Lam, L. Zhang, K. M. Yamada, R. M. Lafrenie, *J Cell Physiol* **2001**, 189, 79.

[34] F. Li, Y. Zhang, C. Wu, *Journal of Cell Science* **1999**, 112, 4589.

[35] K. Fukuda, S. Gupta, K. Chen, C. Wu, J. Qin, *Molecular Cell* **2009**, 36, 819.

[36] P. C. McDonald, S. Dedhar, *Cancers (Basel)* **2022**, 14.

[37] A. N. Kilinc, S. Han, L. A. Barrett, N. Anandasivam, C. M. Nelson, *Mol Biol Cell* **2021**, 32, 402.

[38] M. Hu, X. Li, W.-P. Huang, D.-F. Hu, K.-F. Ren, J. Ji, *Science China Materials* **2021**, 64, 2580.

[39] S. C. Allen, J. A. Widman, A. Datta, L. J. Suggs, *Integrative Biology* **2020**, 12, 161.

[40] M. H. Joyce, C. Lu, E. R. James, R. Hegab, S. C. Allen, L. J. Suggs, A. Brock, *Front Oncol* **2018**, 8, 337.

[41] a)M. A. Feitelson, A. Arzumanyan, R. J. Kulathinal, S. W. Blain, R. F. Holcombe, J. Mahajna, M. Marino, M. L. Martinez-Chantar, R. Nawroth, I. Sanchez-Garcia, D. Sharma, N. K. Saxena, N. Singh, P. J. Vlachostergios, S. Guo, K. Honoki, H. Fujii, A. G. Georgakilas, A. Bilsland, A. Amedei, E. Niccolai, A. Amin, S. S. Ashraf, C. S. Boosani, G. Guha, M. R. Ciriolo, K. Aquilano, S. Chen, S. I. Mohammed, A. S. Azmi, D. Bhakta, D. Halicka, W. N.

Keith, S. Nowsheen, *Semin Cancer Biol* **2015**, 35 Suppl, S25; b)J. Sjöström, J. Bergh, *Bmj* **2001**, 322, 1538.

[42] J. Wei, J. Yao, C. Yang, Y. Mao, D. Zhu, Y. Xie, P. Liu, M. Yan, L. Ren, Y. Lin, Q. Zheng, X. Li, *Journal of Translational Medicine* **2022**, 20, 555.

[43] J. Dittmer, *Semin Cancer Biol* **2017**, 44, 72.

[44] A. Recasens, L. Munoz, *Trends Pharmacol Sci* **2019**, 40, 128.

[45] a)R. V. Kondapaneni, L. A. Shevde, S. S. Rao, *Adv Biol (Weinh)* **2023**, 7, e2200114; b)A. A. Narkhede, J. H. Crenshaw, D. K. Crossman, L. A. Shevde, S. S. Rao, *Acta Biomater* **2020**, 107, 65.

[46] a)S. Persad, S. Attwell, V. Gray, M. Delcommenne, A. Troussard, J. Sanghera, S. Dedhar, *Proc Natl Acad Sci U S A* **2000**, 97, 3207; b)Y. Qu, C. Hao, J. Xu, Z. Cheng, W. Wang, H. Liu, *Mol Med Rep* **2017**, 16, 5036; c)M.-F. Pang, M. J. Siedlik, S. Han, M. Stallings-Mann, D. C. Radisky, C. M. Nelson, *Cancer research* **2016**, 76, 5277.

[47] a)X. Qin, X. Lv, P. Li, R. Yang, Q. Xia, Y. Chen, Y. Peng, L. Li, S. Li, T. Li, Y. Jiang, H. Yang, C. Wu, C. Zheng, J. Zhu, F. You, H. Wang, J. Chen, Y. Liu, *Biochimica et Biophysica Acta (BBA) - Molecular Basis of Disease* **2020**, 1866, 165625; b)J. L. Sacco, Z. T. Vaneman, E. W. Gomez, *J Cell Physiol* **2023**.

[48] J. Yang, Y. Hou, M. Zhou, S. Wen, J. Zhou, L. Xu, X. Tang, Y.-e. Du, P. Hu, M. Liu, *The International Journal of Biochemistry & Cell Biology* **2016**, 71, 62.

[49] H. Shen, J. L. Ma, Y. Zhang, G. L. Deng, Y. L. Qu, X. L. Wu, J. X. He, S. Zhang, S. Zeng, *World J Gastroenterol* **2016**, 22, 3969.

[50] B. Diop-Frimpong, V. P. Chauhan, S. Krane, Y. Boucher, R. K. Jain, *Proceedings of the National Academy of Sciences* **2011**, 108, 2909.

[51] C. Vennin, T. Chin Venessa, C. Warren Sean, C. Lucas Morghan, D. Herrmann, A. Magenau, P. Melenec, N. Walters Stacey, G. del Monte-Nieto, R. W. Conway James, M. Nobis, H. Allam Amr, A. McCloy Rachael, N. Currey, M. Pinese, A. Boulghourjian, A. Zaratzian, A. S. Adam Arne, C. Heu, M. Nagrial Adnan, A. Chou, A. Steinmann, A. Drury, D. Froio, M. Giry-Laterriere, L. E. Harris Nathanial, T. Phan, R. Jain, W. Weninger, J. McGhee Ewan, R. Whan, L. Johns Amber, S. Samra Jaswinder, L. Chantrill, J. Gill Anthony, M. Kohonen-Corish, P. Harvey Richard, V. Biankin Andrew, n. null, T. R. J. Evans, I. Anderson Kurt, T. Grey Shane, J. Ormandy Christopher, D. Gallego-Ortega, Y. Wang, S. Samuel Michael, J. Sansom Owen, A. Burgess, R. Cox Thomas, P. Morton Jennifer, M. Pajic, P. Timpson, *Science Translational Medicine* **2017**, 9, eaai8504.

[52] a)B. Ananthanarayanan, Y. Kim, S. Kumar, *Biomaterials* **2011**, 32, 7913; b)J. A. Burdick, C. Chung, X. Jia, M. A. Randolph, R. Langer, *Biomacromolecules* **2005**, 6, 386.

[53] a)A. Khanlari, J. E. Schulteis, T. C. Suekama, M. S. Detamore, S. H. Gehrke, *Journal of Applied Polymer Science* **2015**, 132; b)A. M. Rosales, S. L. Vega, F. W. DelRio, J. A. Burdick, K. S. Anseth, *Angewandte Chemie International Edition* **2017**, 56, 12132.